Research in
Astronomy and
Astrophysics

Polarization Studies in Different Blazar Types. Part I: Correlation between Optical Brightness and Polarization Degree

E. A. Shkodkina[1], S. S. Savchenko[1,2], D. A. Morozova[1], S. G. Jorstad[1,3], G. A. Borman[4],
T. S. Grishina[1], E. N. Kopatskaya[1], E. G. Larionova[1], A. A. Vasilyev[1], I. S. Troitskiy[1],
Yu. V. Troitskaya[1], P. A. Novikova[1], E. V. Shishkina[1] and A. V. Zhovtan[4]

[1] Saint Petersburg State University, 7/9 Universitetskaya nab., St. Petersburg, 199034 Russia.;
   shkodkina.e.a@gmail.com
[2] Central (Pulkovo) Astronomical Observatory, Russian Academy of Sciences, St. Petersburg, 196140,
   Russia
[3] Institute for Astrophysical Research, Boston University, 725 Commonwealth Avenue, Boston, MA
   02215, USA
[4] Crimean Astrophysical Observatory RAS, P/O Nauchny, 298409, Russia

Abstract We present an analysis of the cross-correlation between optical brightness and polarization degree in different types of blazars. The aim is to identify objects with simultaneous and consistent changes in characteristics and to determine if this behavior relates to the types of objects studied. The analysis includes 23 objects: 11 FSRQ, 11 BL Lac, and 1 radio galaxy. Dense overlapping observation series in the *R* band were used, collected over more than 10 years as part of a monitoring program for bright blazars at St. Petersburg State University. The cross-correlation analysis procedure is detailed, including a method for assessing significance based on Monte Carlo simulations of synthetic light curves modeled using a Damped Random Walk. Significant correlations were found for 5 FSRQ and 1 BL Lac. No significant correlation was detected for 10 BL Lac and 6 FSRQ. One object did not yield a reliable estimate. Based on the current results, we cannot claim that the observed difference in the behavior of these emission characteristics for different classes of blazars is significant. It is possible that observed correlations may be explained by the contribution of simultaneous flare events to the changes in flux and polarization degree curves, which occur more frequently in FSRQ objects.

Key words: galaxies: active — BL Lacertae objects: general — polarization — methods: data analysis

1 INTRODUCTION

Blazars are a class of Active Galactic Nuclei (AGN) with extremely bright, variable emission, dominating over the host galaxy. Variability occurs on timescales from minutes to decades (Hufnagel & Bregman 1992). Unified models suggest this emission originates from a relativistic jet pointed at a small angle to the observer, resulting in relativistic beaming (Blandford et al. 1978). Blazars are divided into FSRQs (Flat Spectrum Radio Quasars) and BL Lac objects, which differ in their optical spectra (Urry & Padovani 1995). FSRQs show strong, broad emission lines, while BL Lac objects have weak or no lines.

Blazar spectral energy distributions feature two components: a low-energy one peaking in the optical, ultraviolet, or X-ray range, and a high-energy one peaking in the gamma range. Both are considered non-thermal. The low-frequency component is attributed to synchrotron radiation from relativistic electrons in the jet's magnetic field (Marscher et al. 2008). It is believed that the synchrotron nature causes high polarization, with degrees up to 50% (Mead et al. 1990). However, many details of the variable polarized emission generation mechanisms in blazars remain unclear.

A variety of jet models have been proposed to explain the observed blazar emission variability. These include models based on chaotic magnetic fields compressed by shock waves (Laing 1980; Angelakis et al. 2016), helical jets with helical magnetic fields (Raiteri et al. 2013), somehow related to the spin of the central black hole (Chen et al. 2024), and models involving knots moving in a toroidal magnetic field (Marscher et al. 2010). Other models consider magnetic field line reconnection, leading to energy release and particle acceleration on short time-scales (Sironi & Spitkovsky 2014). A model for large-scale flux variations involves changes in Doppler boosting due to temporal variations in the jet viewing angle (Raiteri et al. 2017). Models based on turbulent emitting cells in jets are also used to explain the chaotic variability of polarized emission (Marscher 2014).

Studying the variability of polarized emission is an accessible way to obtain information about the magnetic field, its role in particle acceleration, its interaction with the surrounding environment, and its relation to overall emission. Examining the connection between events with high and low polarization can provide understanding of the central regions' structure and the processes occurring within them.

Many studies have focused on analyzing the relationship between the degree of polarization and total flux. For example, in Raiteri, C. M. et al. (2012); Itoh et al. (2018); Otero-Santos et al. (2023) correlated evolution of the polarization degree and the total flux was reported for different objects. In other cases, an anticorrelation was observed (Fraija et al. 2017; Pandey et al. 2022; Rajput et al. 2022; Bachev et al. 2023). Also no relationship was found (Covino et al. 2015; Itoh et al. 2018; Otero-Santos et al. 2023). The data and processing methods used in each of these studies differed significantly, which may contribute to the variability in the reported findings.

This work focuses on studying the correlation between variations in the polarization degree and brightness in the optical spectrum for various types of blazars. We analyze long observation series, with particular emphasis on the methods used for cross-correlation analysis. The structure of the paper is as follows: Section 2 provides a description of the sample and observation process. Section 3 explains the methodology applied for data analysis. The main results and discussion are presented in Sections 5 and 6, respectively.

2 SAMPLE AND OBSERVATIONS

In this work, we study gamma-ray bright blazars included in the observational program at Saint Petersburg State University[1]. We possess extended observational series compiled from data obtained by various telescopes, as detailed below. Observations spanning 10 years or more provide unique datasets with long durations and dense measurements of polarization characteristics for most of the objects included.

A total of 23 objects were considered in the study: 11 FSRQ-type, 11 BL Lac-type and 1 radio galaxy (RG). For these objects, there are overlapping optical observations of polarization characteristics and total flux. Types of objects (according to those specified in the monitoring program and their main characteristics (according to NASA/IPAC Extragalactic Database[2]) are listed in Table 1. Information about the optical total and polarized flux observations are provided in Table 2.

We combine optical photometric and polarimetric data obtained using following telescopes: LX-200 ($40\,\text{cm}$, Saint Petersburg State University, Peterhof), AZT-8 ($70\,\text{cm}$, Crimean Astrophysical Observatory, Nauchny), Perkins ($1.83\,\text{m}$, Perkins Telescope Observatory, Flagstaff, AZ, USA), and the Kuiper and Bok telescopes ($1.54\,\text{m}$ and $2.29\,\text{m}$, respectively, Steward Observatory, Tucson, AZ, USA).

---

[1] https://vo.astro.spbu.ru/program_all/
[2] http://ned.ipac.caltech.edu/

Table 1: Information about the objects.

Name	Type	RA (J2000)	DEC (J2000)	z
3C 66a	BLLac	02 22 39.6	+43 02 08	0.370000
OJ 049	BLLac	08 31 48.9	+04 29 39	0.173856
Mkn 421	BLLac	11 04 27.3	+38 12 32	0.030021
S4 0954+65	BLLac	09 58 47.2	+65 33 55	0.369400
BL Lacertae	BLLac	22 02 43.3	+42 16 40	0.066800
OJ 287	BLLac	08 54 48.9	+20 06 31	0.305600
PG 1553+11	BLLac	15 55 43	+11 11 24	0.360000
PKS 0735+17	BLLac	07 38 07.4	+17 42 19	0.424000
Q 1959+65	BLLac	19 59 59.8	+65 08 54	0.047000
S5 0716+71	BLLac	07 21 53.4	+71 20 36	0.310000
W Com	BLLac	12 21 31.7	+28 13 59	0.102000
AO 0235+16	FSRQ	02 38 38.9	+16 36 59	0.940000
3C 454.3	FSRQ	22 53 57.7	+16 08 54	0.859000
OJ 248	FSRQ	08 30 52.1	+24 11 00	0.938770
CTA 102	FSRQ	22 32 36.4	+11 43 51	1.032000
3C 273	FSRQ	12 29 06.7	+02 03 09	0.158339
3C 279	FSRQ	12 56 11.1	-05 47 22	0.536200
CTA 26	FSRQ	03 39 31	-01 46 36	0.852000
PKS 0420-01	FSRQ	04 23 15.8	-01 20 33	0.916090
Q 0836+71	FSRQ	08 41 24.3	+70 53 42	2.172000
Q 1156+29	FSRQ	11 59 31.8	+29 14 44	0.724745
PKS 1222+21	FSRQ	12 24 54.4	+21 22 46	0.433826
3C 84	RG	03 19 48.2	+41 30 42	0.017559

Table 2: Information about the optical total and polarized flux observations.

Name	R			Polarization Degree		
	Num. points	Length (days)	Mean Cadence (days)	Num. points	Length (days)	Mean Cadence (days)
3C 66a	1902	6390.41	3.36	2170	6390.41	2.95
OJ 049	429	5793.17	13.54	429	5793.17	13.54
Mkn 421	1677	4712.49	2.81	2121	5187.93	2.45
S4 0954+65	2016	6590.11	3.27	2028	6590.11	3.25
BL Lacertae	6200	6563.94	1.06	6553	6563.94	1.00
OJ 287	2569	6606.06	2.57	2953	6606.06	2.24
PG 1553+11	688	3213.14	4.68	741	3213.14	4.34
PKS 0735+17	671	6354.71	9.48	710	6354.71	8.96
Q 1959+65	716	5420.06	7.58	844	5420.06	6.43
S5 0716+71	4983	6568.12	1.32	5204	6568.12	1.26
W Com	881	6606.0	7.51	1143	6606.0	5.78
AO 0235+16	989	6245.32	6.32	1151	6245.32	5.43
3C 454.3	2159	5870.36	2.72	2622	5870.36	2.24
OJ 248	383	5788.43	15.15	521	5788.43	11.13
CTA 102	2167	6410.1	2.96	2310	6410.1	2.78
3C 273	509	5847.43	11.51	747	5847.43	7.84
3C 279	1845	5852.0	3.17	2188	5852.0	2.68
CTA 26	409	5885.3	14.42	431	5885.3	13.69
PKS 0420-01	434	6546.48	15.12	447	6546.48	14.68
Q 0836+71	402	5800.51	14.47	407	5800.51	14.29
Q 1156+29	1482	6815.58	4.60	1552	6815.58	4.39
PKS 1222+21	803	5591.46	6.97	1105	5591.46	5.06
3C 84	301	3697.56	12.33	301	3697.56	12.33

Measurements at the LX-200 telescope were carried out without a filter until late 2018, with a central wavelength of $\lambda_{\mathrm{eff}} = 6700$ Å; afterward, the R filter was used. The instrumental polarization

was measured using stars located near the object in the celestial sphere, assuming that the radiation from the calibration stars is unpolarized. Generally, the measurement errors in the polarization degree do not exceed 1% for objects with a magnitude of $\sim 17^m$. The typical total exposure times (summed over several individual exposures) range from $100\,\mathrm{s}$ for bright objects to $1500\,\mathrm{s}$ for faint ones. Median polarization degree for objects in our sample is 7.9%, with the values 15.2% for the object 3C 279 with typically high polarization degree and 0.3% for the 3C 273 with typically low polarization degree.

The observations at Steward Observatory were performed using the CCD Imaging/Spectro-polarimeter (SPOL; Schmidt et al. (1992)), yielding spectra from $4000\,\text{Å}$ to $7550\,\text{Å}$. The spectra were used to calculate the linear polarization parameters within $5000 - 7000\,\text{Å}$, close to R band. The majority of spectra were accompanied by photometric measurements in the V band (Schmidt et al. 1992), which are not included in our study, as we aim to ensure data uniformity and focus on the analysis of brightness in the R filter specifically. Some Steward data provide the total flux density in R band; V photometry was used to normalize spectra and then from a spectrum the brightness in R band. Observations at other instruments were conducted in the R filter.

Detailed information on the methodology for collecting and processing observations from the LX-200 and AZT-8 telescopes is available in Larionov et al. (2008), for the Perkins telescope in Jorstad et al. (2010) and for the Steward observatory monitoring programm in Smith et al. (2009).

3 ANALYSIS METHODS

For the cross-correlation analysis, we use the Local Discrete Correlation Function (LDCF) — a mod-ification of the Discrete Correlation Function Edelson & Krolik (1988) algorithm with local normal-ization as proposed by Welsh (1999). Additionally, we provide an assessment of the significance of cross-correlation. A commonly used method is to calculate confidence intervals via Monte Carlo (MC) simulations of the light curves. In the current study, we propose using the Damped Random Walk (DRW) model for simulating the light curves.

3.1 Cross-Correlation Estimation

The Cross Correlation Function (CCF) quantifies the statistical relationship between two variables over time. It is commonly used to determine the similarity between two time series on different time shifts (also often referred as lags). CCF of two real stationary stochastic processes is defined as:

$$R_{XY}(\tau) = \frac{\mathbb{E}[(x(t) - \mu_X)(y(t + \tau) - \mu_Y)]}{\sigma_X \sigma_Y},$$

where $\mathbb{E}[.]$ is the expected value, τ is the time lag, and $x(t)$ and $y(t)$ are realizations of the processes $X(t)$ and $Y(t)$. The means and standard deviations are μ_X, μ_Y and σ_X, σ_Y, respectively. The function is normalized so that R_{XY} takes values between $[-1; 1]$.

In practical applications, finite discrete realizations of random processes are typically observed. To estimate sample cross-correlation in discrete cases, various approximations of this definition are used. The cross-correlation estimation for stationary time series $x(t)$ and $y(t)$, whose values are uniformly distributed over time as $t_n = (n - 1)\Delta t$, where $n = 1, 2, \ldots, N$, can be expressed as:

$$r_{xy}(\tau_k) = \frac{\frac{1}{N^*} \sum\limits_{n=1}^{N} (x_n - \bar{x})(y_{n+k} - \bar{y})}{\sqrt{\frac{1}{N} \sum\limits_{n=1}^{N} (x_n - \bar{x})^2 \frac{1}{N} \sum\limits_{n=1}^{N} (y_n - \bar{y})^2}}.$$

In this case, the lag takes only discrete values $\tau_k = k\Delta t$, where $k \in \mathbb{Z}$. Here, $\bar{x}$ and $\bar{y}$ are the sample means of $x(t)$ and $y(t)$. The coefficient $\frac{1}{N^*}$ may be equal $\frac{1}{N}$ or $\frac{1}{N-k}$, depending on chosen approxi-mation (Welsh 1999). Although such estimation is correct, it is often impractical for real time series,

which may be non-stationary, have measurement errors and irregular discretization. Additionally, measurement errors can vary due to changing conditions, emphasizing the need for methods that provide reliable estimates under these circumstances.

Various methods exist for estimating the correlation of uneven time series. Some researchers also estimate the cross-correlation of simultaneous series using the Spearman rank correlation coefficient. More universal mothods can be grouped into several categories: data interpolation, temporal data binnig, and Fourier transforms. All based on the assumption of series stationarity. In reality, assumptions about stationarity are almost always violated during extended observations of many real processes. This is particularly true for objects such as blazars, which can transition between active and quiescent states. Nevertheless, in the absence of alternative tools, researchers are often forced to overlook this assumption.

We performed a stationarity check on our data using the simple Dickey-Fuller test. For the R band light curves of the objects 3C 273, 3C 84, CTA 102, Mkn 421, OJ 248, PKS 0735+17, and Q 1959+65, we failed to confirm stationarity. It is important to note that this test is not suitable for assessing the stationarity of uneven time series, so these results must be treated with particular caution. However, we lack alternative methods for analyzing uneven time series that do not require interpolation or more complex data transformations. We believe that we can still perform cross-correlation procedure, but it is important to approach the interpretation of the results with caution.

Our data consist of unevenly sampled time series with gaps and measurement uncertainties. For some objects, we have dense, accurate series, while for others, the observations are irregular and error-prone. In some cases, we also lack of photometric observations in R band from the Steward monitoring program. Therefore, we need a cross-correlation estimation method that provides reliable results in such case. As noted by Peterson (1993), interpolation-based methods may fail with highly irregular sampling, and the commonly used ICCF method also does not account for measurement errors (Peterson et al. 1998). Fourier-based methods require data manipulation and mathematically complicate transitions.

In our view, a reasonable choice in the current situation is the LDCF algorithm, which accounts for measurement errors and provides a more reliable, though conservative, estimate (Peterson 1993). This method, along with the assessment of the significance algorithm used in this work, also avoids the need for transitioning to the frequency domain.

3.1.1 Local Discrete Correlation Function

In general, two data sets of different sizes are considered: time-ordered sequences of triples $X = \{t_{xi}, x_i, e_{xi}\}_{i=1}^{N}$ and $Y = \{t_{yj}, y_j, e_{yj}\}_{j=1}^{K}$. Each triple includes the observation time, the measured value, and its uncertainty. For every time lag τ an estimate of CCF for X and Y can be calculated:

$$\text{LDCF}(\tau) = \frac{1}{M} \sum \frac{(x_i - \bar{x}_\tau)(y_j - \bar{y}_\tau)}{\sqrt{|(\sigma_{x\tau}^2 - e_{xi}^2)(\sigma_{y\tau}^2 - e_{yj}^2)|}}.$$

Lag τ lies in the center of a time interval Δt with an arbitrary width. The sum is taken over M pairs of indices (i, j) for which $\tau - \frac{\Delta t}{2} < \Delta t_{ij} < \tau + \frac{\Delta t}{2}$. The average values $\bar{z}_\tau$ and standard deviations $\sigma_{z\tau}$ are calculated only for the points within the corresponding time interval Δt. The resulting cross-correlation function values are limited to the interval [-1, 1].

The choice of time interval width Δt represents a compromise between achieving an accurate estimate of the cross-correlation function and maintaining its detail. To obtain a reliable estimate, the number of points in each time interval must be large enough, general estimation is $M \gg 2$ (Edelson & Krolik 1988).

The strength of the method lies in the fact that it requires no additional description or prediction of the time series behavior, using only the values and measurement errors without interpolation or complex transformations. A relative drawback is that numerous data pairs are required in each Δt interval (Peterson 1993). If the sampling of the series under study differs significantly, choosing an appropriate interval width may become challenging. We suggest that these difficulties can be addressed by using

an adaptive selection of time intervals, where the fixed parameter would not be the interval width Δt but rather the required number of point pairs M. In the future, we hope to implement this method and compare the results of such an analysis with those presented here, obtained using fixed time intervals' width.

In this study, we were choosing fixed interval width Δt for each object specifically, according to the sampling characteristic of its observations. In each case $M \gg 100$.

3.2 Significance Assessment

In the case of AGN light curves and polarization measurements, the data points in the time series are not independent. For blazar light curves, this is explained by the presence of flares, with gradual increases and decreases in brightness. The measured value at any given time depends on previous values. This behavior can be described by the DRW model, where the parameter τ_{DRW}, also known as the damping time, reflects the "memory" of the process.

3.2.1 Damped Random Walk

The DRW process, also known as the Ornstein-Uhlenbeck process, has gained popularity in the analysis of astronomical data over the last decade (Ryan et al. 2018; Burke et al. 2021; Yang et al. 2021; Covino et al. 2022; Zhang et al. 2022).

Kelly et al. (2009) have proposed to describe the optical variability of AGN as a random walk, which characterizes their light curves as a gaussian stochastic process with an exponential covariance function

$$S(\Delta t) = \sigma^2_{DRW} \exp\left(-\left|\frac{\Delta t}{\tau_{DRW}}\right|\right), \tag{1}$$

which has two parameters: amplitude of variations σ_{DRW} and the characteristic damping time τ_{DRW}.

In some cases, deviations from the DRW model are observed for real object light curves. However, stochastic process models with a larger number of parameters, such as those assuming variation of an additional parameter to estimate the slope of the Structure Function (SF), as well as models that combine different stochastic processes, do not provide a better fit than a single DRW process (Kelly et al. 2011; Zu et al. 2013).

The works of Kelly et al. (2009); Kozłowski et al. (2010); MacLeod et al. (2010) have shown that the DRW model provides a reasonable explanation for the variability of individual quasars in the Optical Gravitational Lensing Experiment (OGLE) (Udalski et al. 1997) and Sloan Digital Sky Survey (SDSS) Stripe 82 (S82) (Sesar et al. 2007) samples, and that the parameters τ_{DRW} and σ_{DRW} correlate with such physical properties as luminosity and black hole mass. The study of MacLeod et al. (2011) demonstrated that the structure functions of quasars can be recovered by DRW modeling of light curves using estimates of the real physical parameters of the object. Furthermore, the DRW description is used for modeling AGN light curves in the task of reverberation mapping (Zu et al. 2011). Zhang et al. (2022) and Zhang et al. (2023) have also shown that this model is reliable for describing the variability of optical, X-ray, and gamma-ray emissions of blazars.

However, this model is not fully universal and has specific features that must be taken into account. The DRW model does not always provide a good fit between real and modeled data (Kelly et al. 2011). The significance of deviations depends on data uncertainties. Deviations may be significant if the error estimation accuracy is less than 10% and if the error distribution exhibits heavier tails than a normal distribution (Zu et al. 2013). Moreover, studies Kozłowski et al. (2010) and Burke et al. (2021) report that the parameter τ_{DRW} may be incorrectly estimated for data sets that are too short or contain substantial gaps. Similar conclusions are drawn by Zu et al. (2013). Burke et al. (2021) argue that the estimate of τ_{DRW} can be considered reliable if it is greater than the mean cadence of the observations and less than 1/10 of the total duration of the observed light curve. Kozłowski et al. (2010) and Kozłowski (2016) noted that errors in estimating τ_{DRW} are not critical if parameter tuning is not the main goal. This

applies when the DRW model is used only to reconstruct or simulate data, not to estimate physical parameters.

In the current study we are modeling optical light curves of the blazars. For this purpose, we use the JAVELIN[3] package. It was originally designed for reverbation mapping problems and utilizes the DRW process to model blazars light curves. The authors provide a detailed justification for the use of this approach in their works Zu et al. (2011, 2013).

It is important to note that stationarity is also required here, which may be violated in the case of long blazar's light curves. However, modeling non-stationary processes with uneven time sampling is considerably more complex, and therefore, we are compelled to make this assumption.

3.2.2 Confidence Intervals Construction

A comprehensive description of cross-correlation requires an assessment of its statistical significance. Internal correlations between adjacent points in the time series must be taken into account. Correlation measures the linear statistical relationship but does not imply causality between events. For example, when analyzing the correlation between two time series, each showing a flare, the cross-correlation function will exhibit a peak at some time lag, even if the signals are not related.

Standard methods commonly used to assess the significance of correlation assume that individual data points are uncorrelated. In the context of the DRW model, this behavior corresponds to the limiting case of $\tau_{DRW} = 0$. However, for the vast majority of real curves, the τ_{DRW} parameter is significantly different from 0. Ignoring the internal correlation of the data leads to an overestimation of the significance of cross-correlations and erroneous physical interpretations. This effect is demonstrated in Figure 1, where for three simulated pairs of uncorrelated signals with different τ_{DRW} values the cross-correlation function is computed. It can be seen, that for signals with higher values of τ_{DRW} some spurious correlation peaks appear.
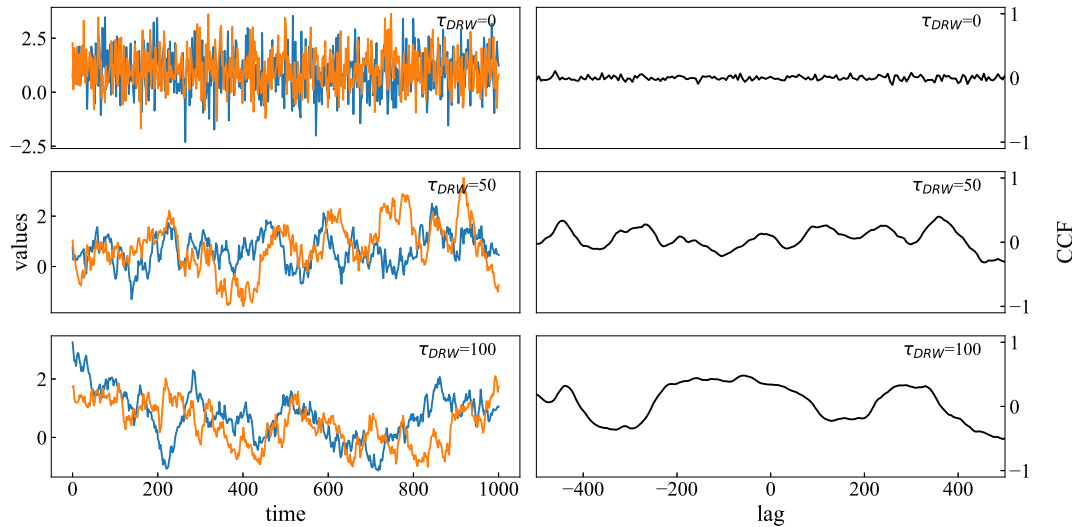
Fig. 1: CCF (right) of two independent signals (left) corresponding to the DRW model with different τ_{DRW}. The signals are defined on a uniform grid without the addition of random error.

A reasonable approach is to use Monte Carlo simulations. Simulating artificial signals and calculating their cross-correlation on the actual time grid with real errors allows for both signal characteristics

---

[3] https://github.com/nye17/javelin

and observational imperfections to be accounted for. This is particularly important in the context of the LDCF method, as the choice of averaging interval width is critically important. If the interval contains too few points for proper averaging, it can lead to inflated/deflated false correlations. Below, Figure 2 illustrates the impact of grid irregularities and measurement errors on the cross-correlation estimation of two time series using the LDCF method. The signals are generated to exhibit identical behavior at lag $= 0$ and have a parameter $\tau_{DRW} = 25$. Gaps and errors were introduced randomly in this case solely to demonstrate the effect. In actual observations, such effects may become even more pronounced.
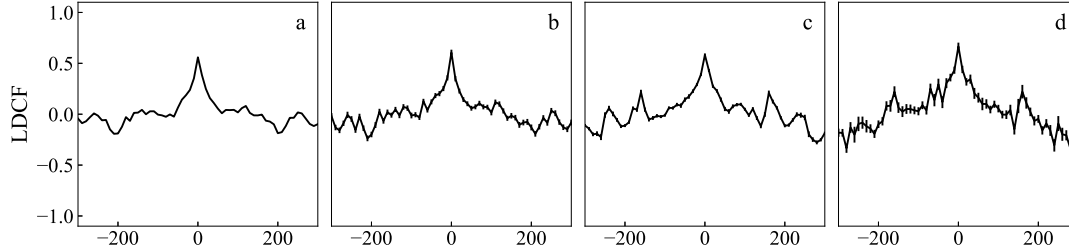
Fig. 2: CCF estimation of two independent signals using LDCF method. (a) signals are generated without random errors, on a uniform grid; (b) signals are generated with random errors, on an irregular grid without significant gaps; (c) signals are generated with random errors, on a grid with large seasonal gaps; (d) signals are generated with random errors, on a grid with large seasonal gaps and additional irregular gaps.

The idea of using Monte Carlo simulations in the context of astronomical data analysis has been discussed and applied by other authors (Edelson et al. 1995; Uttley et al. 2003; Max-Moerbeck et al. 2014). The details of the procedure may vary from study to study. Typically, methods based on power spectrum density or structure function are used to model AGN light curves. However, as noted in Emmanoulopoulos et al. (2010), using structure functions to assess blazar variability comes with several challenges and limitations. The method based on PSD, first proposed in Uttley et al. (2003) and improved in Max-Moerbeck et al. (2014), is more justified but has its downsides. The improved method involves transforming into the frequency domain, which requires complex mathematical transformations and the use of window functions. Moreover, to obtain a smooth periodogram, additional filtering and interpolation in the time domain are necessary. The final technique becomes complex to understand and reproduce. When simulating synthetic curves to construct confidence intervals using such a model, the result depends not only on grid discretization, curve length, and measurement errors but also on the choice of window function.

All these complexities are justified in the context of the challenging task of correlational analysis of irregular time series. However, we aim to find a simpler, more intuitive method that requires fewer manipulations and transformations. Therefore, we explore the possibility of using the DRW model for simulating artificial curves. This approach does not require prior interpolation or data smoothing, nor does it involve transitioning from the time domain to the frequency domain.

The overall scheme of our procedure for estimating cross-correlations and constructing confidence intervals (CIs) is shown below. It can be applied to any curves with an appropriate distribution of data points, e.g., for two light curves. In our case, these are the light (L) and the polarization degree curves (PD).

1. Calculate the cross-correlations of the uneven time series (L and PD) using the selected method.
2. Estimate the parameters τ_{DRW} and σ_{DRW} of the model for one of the analyzed curves (L).
3. Simulate N artificial curves based on the DRW model with the parameters estimated in the previous step and add random errors corresponding to the measurement errors. The artificial (L) curves are defined on the same time grid as the original data.

4. Calculate the cross-correlations of the (PD) curve, for which steps 2-3 were not performed, with each of the N artificial (L) curves. For each pair, the values of the cross-correlation at the corresponding time delay τ are recorded.

5. Assess the significance levels of the cross-correlation coefficients of the original data based on the empirical distribution of the cross-correlation values at each time delay τ. The 2σ and 3σ significance levels correspond to the 95th and 99th percentiles of the obtained distributions.

To estimate the confidence intervals (CIs), we propose simulating only the optical light curves. Since the JAVELIN library we are using was originally developed for optical reverberation mapping, we lack an appropriate tool for modeling polarization degree curves. For these reasons, we focus exclusively on modeling artificial optical light curves. This choice also significantly reduces computation time without violating the conditions of the task. Our approach evaluates the probability that the observed cross-correlation pattern arises by chance, given the current characteristics of the data. The artificial series, modeled using the parameters of one curve, preserve its statistical properties, while the second curve retains its original characteristics.

4 DATA ANALYSIS

The main goal of our research is to analyze the correlations between long-term observational series of optical brightness and polarization degree, corresponding to $lag \approx 0$. In other words, we are interested in identifying objects for which the behaviors of these characteristics are correlated and occur simultaneously or quasi-simultaneously, and whether this correlated behavior is associated with the types of the studied objects.

The cross-correlation was evaluated using the LDCF algorithm. Our choice to conduct cross-correlation analysis specifically on long-term light curves is deliberate. Although some authors report correlations between light curve behavior and optical polarization only during periods of high activity (Pandey et al. 2022; Bachev et al. 2023), this study focuses on the overall analysis of the curves. Such an approach allows for a more reliable reconstruction of the DRW model parameters (Sec. 3.2.1) and the use of DRW curve simulations to estimate CIs.

As previously mentioned, we employed the JAVELIN package for modeling the optical light curves of blazars. Parameter fitting employs a Markov Chain Monte Carlo (MCMC) sampler via the EMCEE[4] package. Further details can be found in Zu et al. (2011, 2013) and the library documentation.

When estimating the parameters of the optical light curves, a uniform distribution is used by default to estimate τ_{DRW} and σ_{DRW} in JAVELIN, but with additional constraints. For both parameters, a uniform distribution with a logarithmic scale is assumed. For σ_{DRW}, a penalty is applied by calculating $-log(\sigma)$. For τ_{DRW}, the penalty is adjusted as follows: if τ_{DRW} exceeds the duration D of the data, the penalty is calculated as $-log(\frac{\tau}{D})$. If τ_{DRW} is less than 0.001, a penalty of $-\infty$ is applied (i.e., this value is considered completely unacceptable). The MCMC sampler was run for 10^5 iterations with 16 parallel walkers exploring the parameter space. The first $3 \cdot 10^3$ steps were used as burn-in. The result of this fitting process is an estimate of the posterior distribution of the parameters along with corresponding highest posterior density intervals. The parameter τ_{DRW} was compared with the limits proposed in Burke et al. (2021): it should be no smaller than the mean cadence and no larger than $1/10$ of the total length of the studied curve.

After parameter estimation, around 10^5 artificial light curves were generated to evaluate the significance of the cross-correlation of the original signals. The number of artificial light curves was set depending on the convergence and computational cost of the generation and confidence interval calculation algorithms. Convergence was assessed by the appearance of the empirical distribution of cross-correlation coefficients, only for the zero time lag.

---

[4] https://emcee.readthedocs.io/en/stable/

5 RESULTS

Below are the results of the cross-correlation values computed using the LDCF method and the estimation of CI for several illustrative cases. The results of cross-correlation evaluations and the parameters of the optical brightness curves σ_{DRW} and τ_{DRW} for all objects are provided in Table 3.

5.1 OJ 248

The light curves of the FSRQ object OJ 248 (Fig. 3) provide a good example of the correlated behavior of the polarization degree and optical brightness. The characteristics exhibit similar behavior, both showing a flare localized in 56000-56500 MJD. The correlation is confirmed by our evaluation — a significant CCF peak is observed at $lag = 0$. The asymmetries of the CIs for this and other cases are due to overall irregularities, seasonal gaps, and the length of the observed curves. This leads to different numbers of point pairs in each averaging interval, which is reflected in the irregular shape of the CI. The estimates of the τ_{DRW} parameter for R curve are consistent with the limits proposed in Burke et al. (2021). A correlation between the optical light curve and degree of polarization curve for this source was also reported by Carnerero et al. (2015), Raiteri & Villata (2021) and Otero-Santos et al. (2023).
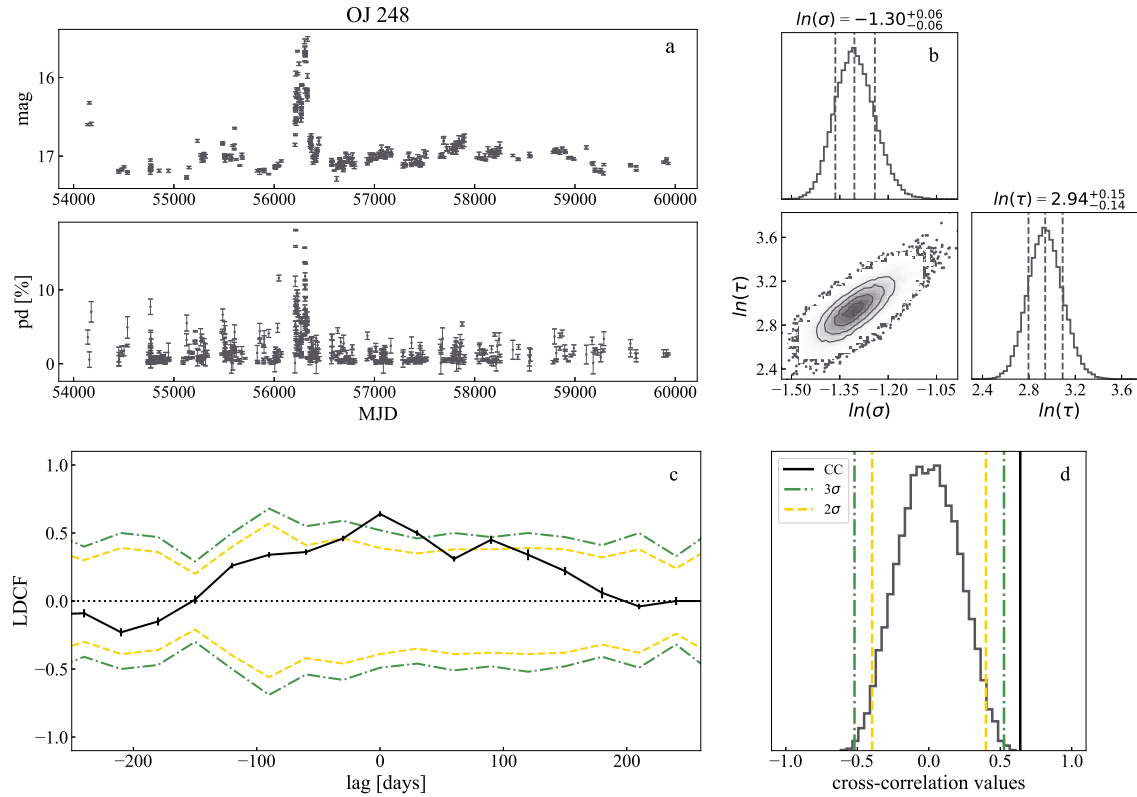
Fig. 3: OJ 248. (a) optical R and PD curves; (b) posterior distribution estimates for σ_{DRW} and τ_{DRW} for R curve; (c) CCF estimation results with CI evaluation; (d) empirical distribution of cross-correlation values obtained from MC simulations for $lag = 0$.

5.2 W Com

The curves of this BL Lac object (see Fig. 4) exhibit uncorrelated behavior between optical brightness and the polarization degree, which is confirmed by our CCF estimation. The estimates of the τ_{DRW} parameter are consistent with the bounds proposed in the study Burke et al. (2021).
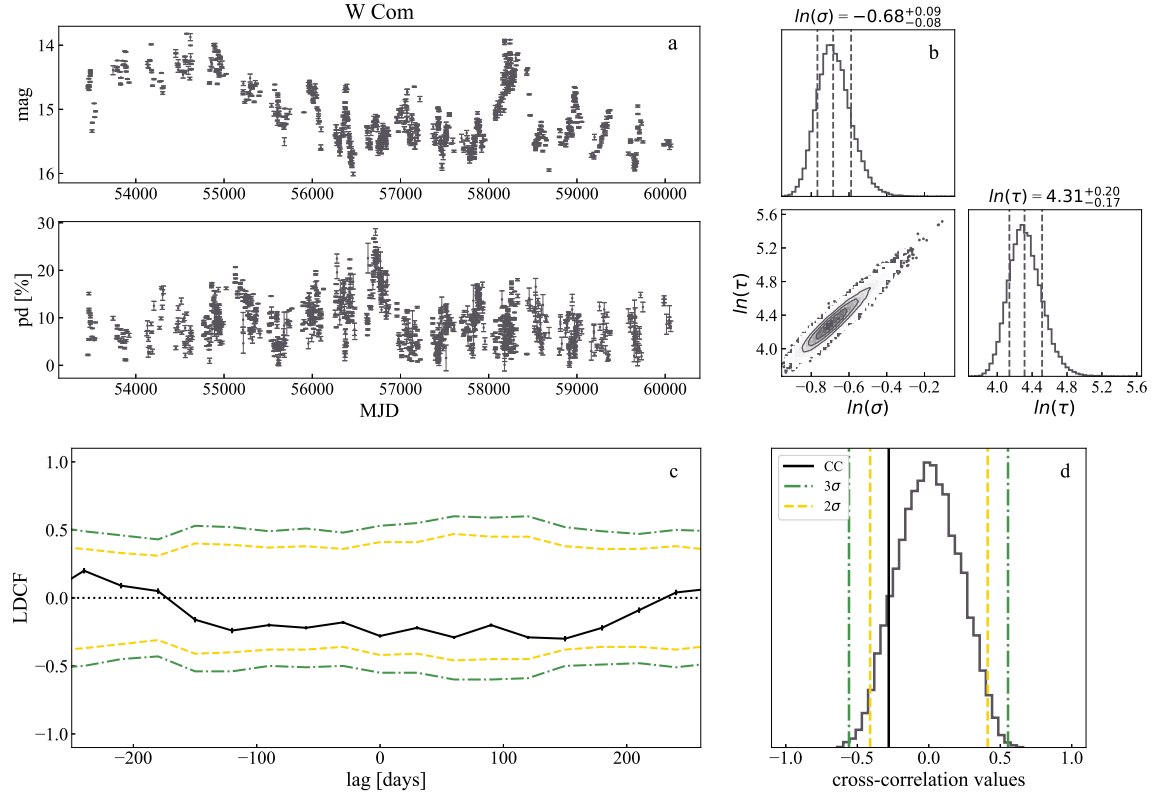
Fig. 4: W Com. (a) optical R and PD curves; (b) posterior distribution estimates for σ_{DRW} and τ_{DRW} for R curve; (c) CCF estimation results with CI evaluation; (d) empirical distribution of cross-correlation values obtained from MC simulations for $lag = 0$.

5.3 3C 84

For this radio galaxy, we were unable to effectively estimate the τ_{DRW} parameter for the light curve or construct a CI estimate (Fig. 5). The resulting estimate of τ_{DRW} is outside the bounds proposed in Burke et al. (2021). The CI limits are too narrow, as if the process describing this object's light curve were almost memory-less. We attribute this to the small number of data points in the light curve and the large measurement errors in the polarization degree. We were unable to improve the parameter estimate by adjusting the settings of the JAVELIN package we used. Unfortunately, the functionality of this library is limited, as it was primarily developed for the task of reverberation mapping. We hope to use a more flexible tool in future studies.
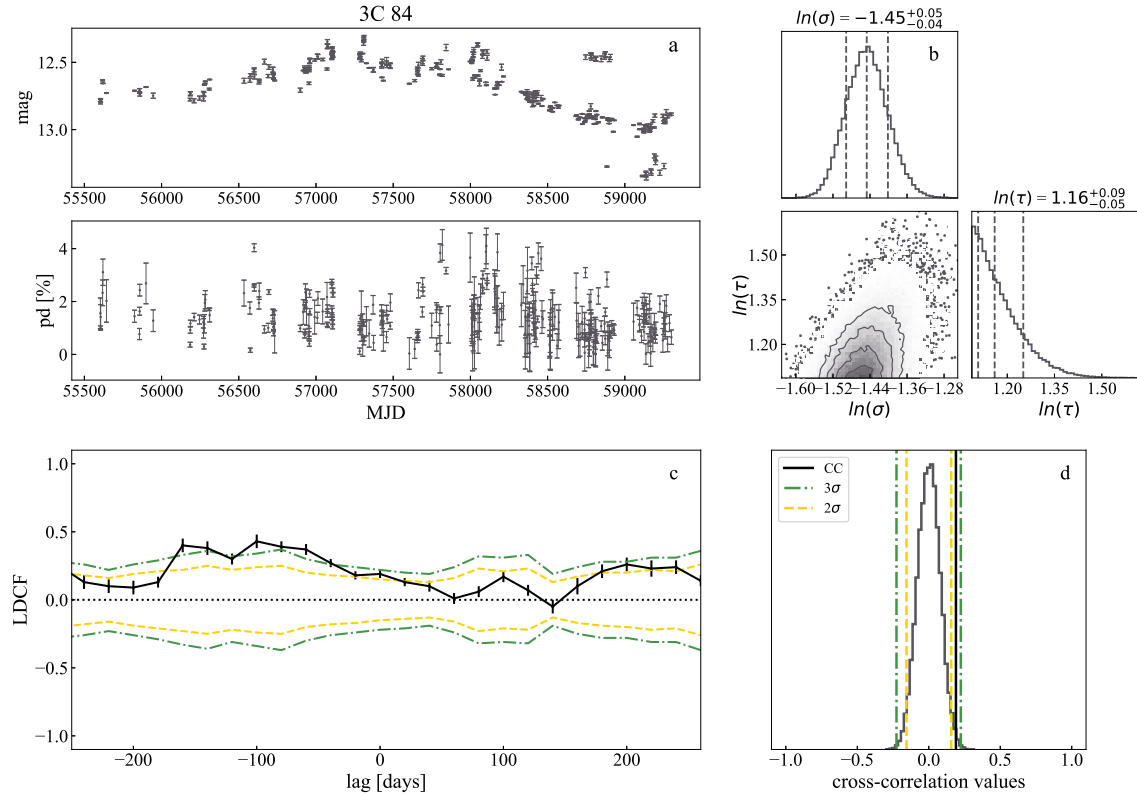
Fig. 5: 3C 84. (a) optical R and PD curves; (b) posterior distribution estimates for σ_{DRW} and τ_{DRW} for R curve; (c) CCF estimation results with CI evaluation; (d) empirical distribution of cross-correlation values obtained from MC simulations for $lag = 0$.

5.4 AO 0235+16

This case illustrates the conservativeness of the cross-correlation estimates we obtained (Fig. 6). For this FSRQ object the cross-correlation estimate at zero lag barely exceed the computed confidence intervals, despite the visually similar behavior of the curves. It is possible that with denser observation series with smaller errors, the correlation could have been confirmed more clearly. The estimates of the τ_{DRW} parameter for R curve are in agreement with the limits proposed in Burke et al. (2021).

5.5 Other Results

All results are presented in Table 3. For 6 objects, we were able to confirm the correlation in the changes of optical brightness and polarization degree. Among them, 5 are FSRQ objects and 1 is a BL Lac object. For 16 objects, we conclude the absence of correlation in the studied curves at zero lag: 10 BL Lac and 6 FSRQ. For the radio galaxy 3C 84, we were unable to obtain a reliable estimate. For PKS 0420-01 and for AO 0235+16, which show visually similar behavior in their curves, the cross-correlation estimates barely exceed 2σ threshold. The result depends on the quantity and density of available observations – for some sources, we may not have sufficient data to reliably characterize the behavior of the studied light curves. Additionally, for the Mkn 421, a noticeable CCF peak exceeding 3σ was observed at $lag \approx 50$ days. However, we cannot be confident in its significance, as the empirical distribution of
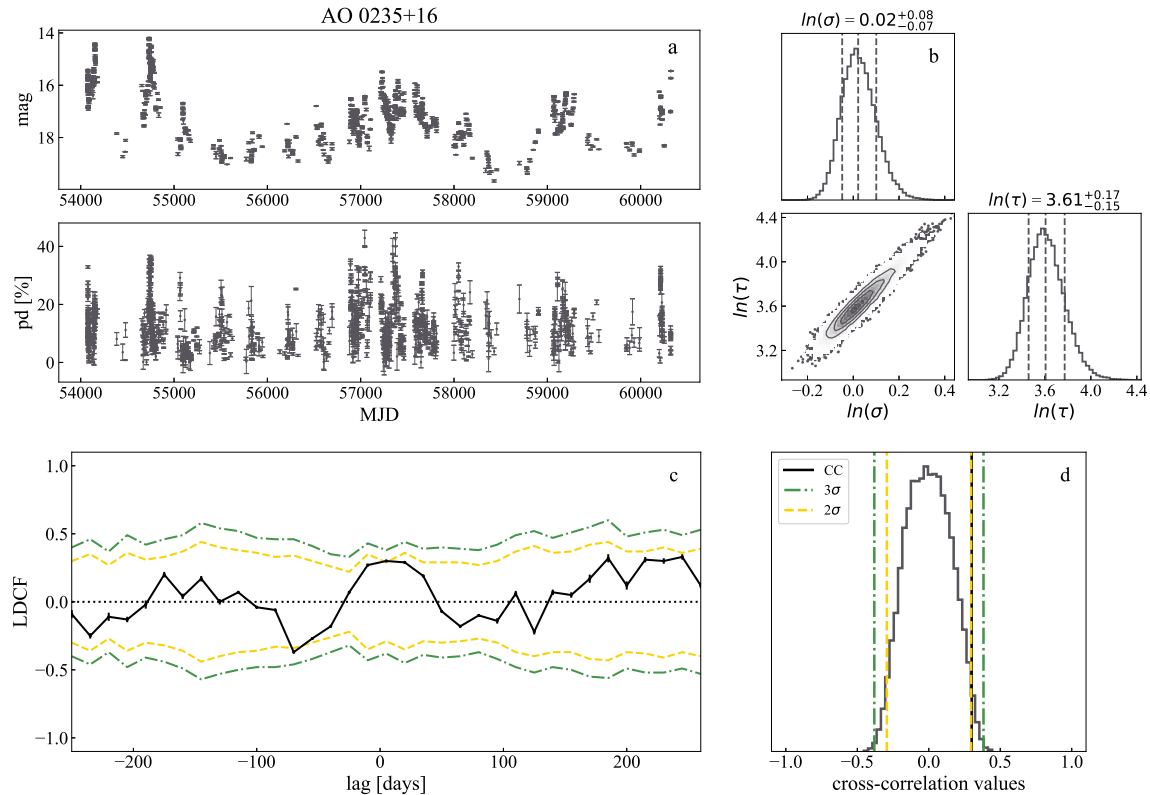
Fig. 6: AO 0235+16. (a) optical R and PD curves; (b) posterior distribution estimates for σ_{DRW} and τ_{DRW} for R curve; (c) CCF estimation results with CI evaluation; (d) empirical distribution of cross-correlation values obtained from MC simulations for $lag = 0$.

cross-correlation coefficients at this lag was not studied. No significant anticorrelation was observed in any of the investigated cases.

6 DISCUSSION AND CONCLUSIONS

We have compared our results with the finding by Otero-Santos et al. (2023), which also focuses on the analysis of long-term blazar observations but uses different methods. The authors report, before correcting the polarization degree for the host galaxy and BLR, a correlation between optical flux and polarization degree observed for 5 of 11 FSRQ objects in their sample, while no correlation is found for BL Lac objects. The sources which reveal a correlated behavior include 4 FSRQs from our study: PKS 0420-01, OJ 248, 3C 454.3, and CTA 102.

The results of our study can be called in agreement with the findings of Otero-Santos et al. (2023). In our sample, 5 out of 6 objects showing significant correlation at zero lag are FSRQ objects. Although, this is not enough to draw definitive conclusions. To test whether the difference in the correlated behavior of the curves between the two types of blazars is significant, we performed a two-sided Fisher's exact test for small binomial samples. The obtained $p - value \approx 0.15$ exceeds the significance level $\alpha = 0.05$, indicating insufficient evidence to reject the null hypothesis (i.e., the samples are equal). Therefore, based on the current data, there is no statistically significant evidence of differences in the emission characteristics between the two blazar classes.

It is possible that the observed correlation between optical flux and polarization degree does not necessarily reflect a stable relationship between these characteristics over the entire observation period,

Table 3: Results.

Name	Correlation (Significance)	τ_{DRW} (days)	σ_{DRW}
3C 66A	N	$102.68^{+126.88}_{-86.03}$	$0.44^{+0.48}_{-0.4}$
OJ 049	N	$16.52^{+19.53}_{-14.21}$	$0.46^{+0.49}_{-0.43}$
Mkn 421	N	$14.65^{+16.34}_{-13.21}$	$0.4^{+0.42}_{-0.38}$
S4 0954+65	Y (2σ)	$14.8^{+16.19}_{-13.61}$	$0.88^{+0.92}_{-0.85}$
BL Lacertae	N	$30.56^{+34.16}_{-27.83}$	$0.65^{+0.68}_{-0.62}$
OJ 287	N	$38.14^{+43.81}_{-33.78}$	$0.53^{+0.57}_{-0.5}$
PG 1553	N	$118.21^{+167.77}_{-89.42}$	$0.28^{+0.33}_{-0.25}$
PKS 0735+17	N	$72.83^{+89.1}_{-60.55}$	$0.59^{+0.65}_{-0.54}$
Q 1959	N	$79.02^{+98.91}_{-65.24}$	$0.32^{+0.35}_{-0.29}$
S5 0716+71	N	$15.53^{+16.83}_{-14.42}$	$0.55^{+0.58}_{-0.53}$
W Com	N	$74.69^{+91.33}_{-62.78}$	$0.5^{+0.55}_{-0.46}$
AO 0235+16	Y (2σ)	$36.82^{+43.46}_{-31.76}$	$1.02^{+1.11}_{-0.95}$
3C 454.3	Y (2σ)	$39.46^{+45.68}_{-34.57}$	$0.73^{+0.79}_{-0.69}$
OJ 248	Y (3σ)	$18.93^{+22.0}_{-16.38}$	$0.27^{+0.29}_{-0.26}$
CTA 102	Y (3σ)	$33.98^{+38.63}_{-30.13}$	$0.86^{+0.92}_{-0.81}$
3C 273	N	$240.16^{+350.6}_{-180.15}$	$0.16^{+0.19}_{-0.14}$
3C 279	N	$47.02^{+55.89}_{-40.4}$	$0.82^{+0.89}_{-0.76}$
CTA 26	N	$33.49^{+40.64}_{-28.01}$	$0.66^{+0.72}_{-0.61}$
PKS 0420-01	Y (2σ)	$88.7^{+112.49}_{-72.33}$	$0.96^{+1.07}_{-0.87}$
Q 0836	N	$13.47^{+16.16}_{-11.28}$	$0.09^{+0.1}_{-0.09}$
Q 1156	N	$54.21^{+64.04}_{-46.71}$	$1.14^{+1.23}_{-1.06}$
PKS 1222+21	N	$145.93^{+196.65}_{-114.93}$	$0.43^{+0.49}_{-0.38}$
3C 84	?	$3.19^{+3.49}_{-3.03}$	$0.24^{+0.25}_{-0.23}$

but is more likely related to the high correlation during individual outbursts. FSRQ objects generally exhibit brighter and more frequent flares compared to BL Lac objects.

The contribution of flares to the observed correlation is especially evident in the case of OJ 248, which demonstrates a single bright flare. For this object, a re-evaluation of the correlation was performed outside the flare state. It was found that the high correlation between examined characteristics disappears during quiescent periods. Similar high correlations for other objects may also be explained by the contribution of simultaneous flare events to the changing flux and polarization degree curves.

The correlation between flare appearances on the flux and polarization degree curves can be explained by shock-in-jet models (Hagen-Thorn et al. 2008; Marscher 1996). In this model, shocks in the jet cause the injection of relativistic electrons into the emission region, leading to a stable spectral shape and short-term variability in the optical range. Furthermore, shocks contribute to the alignment of the magnetic field, resulting in a positive correlation between flux and polarization degree. A similar model is also discussed by Angelakis et al. (2016), describing the differences in the observed optical emission for low-synchrotron peaked (LSP) and high-synchrotron peaked (HSP) objects. Since the optical emission for FSRQ/LSP and ISP/HSP objects is located in different regions of the synchrotron emission curve in the spectral energy distribution, this model explains the higher polarization and variability for the former, compared to the latter. Otero-Santos et al. (2023) also proposed the shock-in-jet model as an explanation for the observed patterns.

Finding more cases of a significant positive correlation between the optical light curve and degree of polarization curve in FSRQs can be a signature of more powerful shocks in quasars than in BL Lac objects. This assumption agrees also with the presumption that the magnetic field energy in BL Lac objects dominates the particle energy even on parsec scales, e.g. for BL Lac itself (Cohen et al. 2014). For a better understanding of the mechanisms leading to the observed features of the emission and

the selection of the most appropriate model, further investigation of other characteristics of polarized emission is required.

We also discussed a method for assessing the significance of cross-correlation in time series, focusing on model selection and problem formulation. Our goal was to find a simple, efficient, and universal approach for evaluating the cross-correlation of uneven time series with various characteristics. While the combination of cross-correlation estimation and confidence interval methods we used performs well, it is computationally demanding and may not be applicable in all cases due to the complexity of the problem. Nevertheless, these methods provide accurate estimates, and we hope to refine the approach and compare it with other correlation estimation and CI calculation methods in the future.

References

Angelakis, E., Hovatta, T., Blinov, D., et al. 2016, Monthly Notices of the Royal Astronomical Society, 463, 3365 2, 14

Bachev, R., Tripathi, T., Gupta, A. C., et al. 2023, Monthly Notices of the Royal Astronomical Society, 522, 3018 2, 9

Blandford, R. D., Rees, M. J., & M., W. A. 1978, Pittsburgh Conference on BL Lac Objects, University of Pittsburgh, Pittsburgh, Pa., April 24-26, 1978, Proceedings (Pittsburgh: University of Pittsburgh) 1

Burke, C. J., Shen, Y., Blaes, O., et al. 2021, Science, 373, 789 6, 9, 10, 11, 12

Carnerero, M. I., Raiteri, C. M., Villata, M., et al. 2015, MNRAS, 450, 2677 10

Chen, Y., Gu, Q., Yang, J., et al. 2024, Research in Astronomy and Astrophysics, 24, 115011 2

Cohen, M. H., Meier, D. L., Arshakian, T. G., et al. 2014, The Astrophysical Journal, 787, 151 14

Covino, S., Tobar, F., & Treves, A. 2022, MNRAS, 513, 2841 6

Covino, S., Baglio, M. C., Foschini, L., et al. 2015, A&A, 578, A68 2

Edelson, R. A., & Krolik, J. H. 1988, ApJ, 333, 646 4, 5

Edelson, R., Krolik, J., Madejski, G., et al. 1995, ApJ, 438, 120 8

Emmanoulopoulos, D., McHardy, I. M., & Uttley, P. 2010, MNRAS, 404, 931 8

Fraija, N., Benítez, E., Hiriart, D., et al. 2017, ApJS, 232, 7 2

Hagen-Thorn, V. A., Larionov, V. M., Jorstad, S. G., et al. 2008, ApJ, 672, 40 14

Hufnagel, B. R., & Bregman, J. N. 1992, ApJ, 386, 473 1

Itoh, R., Uemura, M., Fukazawa, Y., & Kawabata, K. 2018, Galaxies, 6, 16 2

Jorstad, S. G., Marscher, A. P., Larionov, V. M., et al. 2010, ApJ, 715, 362 4

Kelly, B. C., Bechtold, J., & Siemiginowska, A. 2009, ApJ, 698, 895 6

Kelly, B. C., Sobolewska, M., & Siemiginowska, A. 2011, ApJ, 730, 52 6

Kozłowski, S. 2016, The Astrophysical Journal, 826, 118 6

Kozłowski, S., Kochanek, C. S., Udalski, A., et al. 2010, ApJ, 708, 927 6

Laing, R. A. 1980, Monthly Notices of the Royal Astronomical Society, 193, 439 2

Larionov, V. M., Jorstad, S. G., Marscher, A. P., et al. 2008, A&A, 492, 389 4

MacLeod, C. L., Brooks, K., Ivezić, Ž., et al. 2011, The Astrophysical Journal, 728, 26 6

MacLeod, C., Ivezic, Z., Kozlowski, S., et al. 2010, in American Astronomical Society Meeting Abstracts, Vol. 215, American Astronomical Society Meeting Abstracts #215, 433.26 6

Marscher, A. P. 1996, in Astronomical Society of the Pacific Conference Series, Vol. 110, Blazar Continuum Variability, ed. H. R. Miller, J. R. Webb, & J. C. Noble, 248 14

Marscher, A. P. 2014, ApJ, 780, 87 2

Marscher, A. P., Jorstad, S. G., D'Arcangelo, F. D., et al. 2008, Nature, 452, 966 2

Marscher, A. P., Jorstad, S. G., Larionov, V. M., et al. 2010, ApJ, 710, L126 2

Max-Moerbeck, W., Hovatta, T., Richards, J. L., et al. 2014, Monthly Notices of the Royal Astronomical Society, 445, 428 8

Mead, A. R. G., Ballard, K. R., Brand, P. W. J. L., et al. 1990, A&AS, 83, 183 2

Otero-Santos, J., Acosta-Pulido, J. A., Becerra González, J., et al. 2023, MNRAS, 523, 4504 2, 10, 13, 14

Pandey, A., Rajput, B., & Stalin, C. S. 2022, MNRAS, 510, 1809 2, 9

Peterson, B. M. 1993, PASP, 105, 247 5

Peterson, B. M., Wanders, I., Horne, K., et al. 1998, PASP, 110, 660 5

Raiteri, C. M., & Villata, M. 2021, Galaxies, 9 10

Raiteri, C. M., Villata, M., Smith, P. S., et al. 2012, A&A, 545, A48 2

Raiteri, C. M., Villata, M., D'Ammando, F., et al. 2013, MNRAS, 436, 1530 2

Raiteri, C. M., Villata, M., Acosta-Pulido, J. A., et al. 2017, Nature, 552, 374 2

Rajput, B., Pandey, A., Stalin, C. S., & Mathew, B. 2022, MNRAS, 517, 3236 2

Ryan, J. L., Siemiginowska, A., Sobolewska, M., & Grindlay, J. E. 2018, in American Astronomical Society Meeting Abstracts, Vol. 231, American Astronomical Society Meeting Abstracts #231, 205.04 6

Schmidt, G. D., Stockman, H. S., & Smith, P. S. 1992, ApJ, 398, L57 4

Sesar, B., Ivezić, Ž., Lupton, R. H., et al. 2007, AJ, 134, 2236 6

Sironi, L., & Spitkovsky, A. 2014, ApJ, 783, L21 2

Smith, P. S., Montiel, E., Rightley, S., et al. 2009, arXiv e-prints, arXiv:0912.3621 4

Udalski, A., Kubiak, M., & Szymanski, M. 1997, Acta Astronomica, 47, 319 6

Urry, C. M., & Padovani, P. 1995, Publications of the Astronomical Society of the Pacific, 107, 803 1

Uttley, P., Edelson, R., McHardy, I. M., Peterson, B. M., & Markowitz, A. 2003, The Astrophysical Journal, 584, L53 8

Welsh, W. F. 1999, PASP, 111, 1347 4

Yang, S., Yan, D., Zhang, P., Dai, B., & Zhang, L. 2021, ApJ, 907, 105 6

Zhang, H., Yan, D., & Zhang, L. 2022, ApJ, 930, 157 6

Zhang, H., Yan, D., & Zhang, L. 2023, The Astrophysical Journal, 944, 103 6

Zu, Y., Kochanek, C. S., Kozłowski, S., & Udalski, A. 2013, ApJ, 765, 106 6, 7, 9

Zu, Y., Kochanek, C. S., & Peterson, B. M. 2011, ApJ, 735, 80 6, 7, 9